ELSEVIER

Journal of Fluorine Chemistry 107 (2001) 39–44

JOURNAL OF FLUORINE CHEMISTRY

www.elsevier.com/locate/jfluchem

Electrochemical studies of substituted spinel $LiAl_yMn_{2-y}O_{4-z}F_z$ for lithium secondary batteries

Wu Xiaomei[a,*], Zong Xiangfu[a], Yang Qinghe[a], Jin Zhongkao[a], Wu Haoqing[b]

[a]*Institute of Materials Science, Fudan University, 200433 Shanghai, PR China*
[b]*Department of Chemistry, Fudan University, 200433 Shanghai, PR China*

Received 4 May 2000; accepted 24 August 2000

Abstract

To improve the cycle performance of $LiMn_2O_4$ ($Fd\bar{3}m$) as the cathode of 4 V class lithium secondary batteries, the cathode properties of the cubic spinel phases $LiAl_yMn_{2-y}O_{4-z}F_z$ and $LiAl_yMn_{2-y}O_4$ synthesized at 750°C were examined. Although the cycle performance of the $LiAl_yMn_{2-y}O_4$ was improved by the substitution of Al^{3+} for Mn^{3+} in the octahedral sites, the first discharge capacity was reduced considerably compared with that of the parent $LiMn_2O_4$. F-substituted spinel $LiAl_yMn_{2-y}O_{4-z}F_z$ can compensate for the theoretical capacity reduction in $LiAl_yMn_{2-y}O_4$. The X-ray diffraction (XRD) data shows that the single-phase region of y and z in $LiAl_yMn_{2-y}O_{4-z}F_z$ was $0 \leq y \leq 1/12$ and $0 \leq z \leq 0.04$. The shape of the voltammetric peaks in the 2–5 V region and the XRD data suggested that F–Al-substituted spinel can suppress the Jahn–Teller instability to improve the cycling performance better than $LiMn_2O_4$. The above results are further supported by an ac impedance experiment. We compared impedance spectra of the fresh and cycled electrode, measured at potentials close to the SSCV peak potential. The capacity decrease of these electrodes upon cycling is accompanied by a gradual increase in their charge-transfer resistance.

Keywords: Lithium secondary batteries; Spinel; Substitute; Jahn–Teller distortion

1. Introduction

In recent years, the normal spinel $LiMn_2O_4$ has been studied extensively as the cathode for rechargeable lithium cells, because it has such advantages as low cost, low toxicity, relatively high energy density, etc. [1–4]. It is also a candidate to replace $LiCoO_2$. The discharge curve of $Li_xMn_2O_4$ mainly exhibits two voltage plateaus, 4 V for $0 < x \leq 1$ and 3 V for $1 \leq x < 2$, respectively. In 3 V range, a drastic capacity loss with cycling is caused by a large volumetric change with a structural phase transition from cubic to tetragonal, which is derived from the Jahn–Teller distortion of $Mn^{3+}(3d^4)$. Accordingly, it can be cycled only at 4 V range, though a marked capacity fade is still observed.

To improve the cycle performance in 4 V range, several research groups have investigated the properties of manganese-substituted spinels $LiM_yMn_{2-y}O_4$ (M = Al, Cr, Ga, Ti, Ge, Fe, Co, Zn, Ni, Mg) [5–11]. Gummow et al. [7] have pointed out that the substitution of a monovalent or multivalent metal cation for Mn enhances the stability of a spinel. Although the cycle performance of the $LiM_yMn_{2-y}O_4$ was improved by the substitution of M for Mn^{3+} in the octahedral sites, the first discharge capacity was reduced considerably compared with that of the parent $LiMn_2O_4$. Substitution of Mn by M reduces the capacity of the spinel for lithium in 4 V region since these M ions are not oxidized or reduced in this potential range. Recently, Amatucci et al. [12,13] have shown that the introduction of anion substitution in the form of spinel oxyfluorides can reduce the Mn oxidation state and improves the chemical and structural stability of the spinel.

We here investigated a new F- and Al-substituted spinel $LiAl_yMn_{2-y}O_{4-z}F_z$ to compensate for the theoretical capacity reduction in $LiAl_yMn_{2-y}O_4$. Based on the fundamentals of cooperative Jahn–Teller distortion, Al^{3+} was chosen to substitute Mn on the 16*d* sites. Aluminum has a small ionic size (0.53 Å), the small size restricts the dynamic Jahn–Teller Mn^{3+} cations from forming a cooperative *c*/*a* expansion. Aluminum is lightweight, therefore improving specific capacity. The aluminum cation is trivalent allowing greater substitution than Li^+ on the 16*d* sites while retaining Mn^{3+} content critical for retention of capacity. Aluminum is extremely stable in an octahedral environment and allows the maximization of substitution.

* Corresponding author.

0022-1139/01/$ – see front matter
PII: S0022-1139(00)00344-4

2. Experimental

The spinels $LiMn_2O_4$, $LiAl_yMn_{2-y}O_4$ and $LiAl_yMn_{2-y}O_{4-z}F_z$ were prepared by the melt-impregnation method [14] mixing of LiOH, LiF, MnO_2 and Al_2O_3 in stoichiometric quantities. Samples were preheated at 500°C for 6 h, and then annealed in air at 750°C for 2 days with intermittent grindings, followed by slow cooling at a rate of 0.50°C min^{-1}.

The stoichiometry was confirmed by atomic absorption spectrometry and chemical composition analysis. We found that there is almost no significant difference between expected and final composition [15]. X-ray diffraction (XRD) data were collected with a Rigaku 2077 X-ray diffractometer using Cu Kα radiation.

The composite cathode electrodes were made from the spinel sample powders (80% by weight), acetylene black (10% by weight), and polyvinylidene fluoride (PVDF) binder (10% by weight) in *N*-methyl pyrrolidinone (NMP) and then coated uniformly on a 1 cm × 1 cm nickel net. After being dried at 140°C in vacuum, electrodes were pressed at about 1×10^3 kg cm^{-2} pressure. A typical electrode contained ca. 5 mg active material. The electrolyte was 1 M $LiPF_6$ in ethylene carbonate and dimethyl carbonate solution (EC + DMC) (1:1).

The charge and discharge capacities were measured using a coin cell, in which a lithium metal sheet was used as the counter electrode. The coin cell was cycled under constant-current conditions (current density (CD): 0.2 mA cm^{-2}, cut-off voltage 4.3 V for charge, 3.5 V for discharge) at room temperature.

A three-electrode cell was employed for the impedance measurements and slow speed cyclic voltammetry (SSCV), in which lithium foil was used as both the anode and the reference electrode. The cell was not equipped with a separator that might have influenced the ac impedance response of this type of the electrode. The ac frequency was scanned from 65 kHz to 1 mHz with an ac voltage signal of ±5 mV. The measurements were carried out under open circuit voltage (OCV) conditions before and after the constant current (0.2 mA cm^{-2}), charging and discharging at room temperature. Equilibrium was considered to be reached when the open-circuit voltage remained stable (1 mV over 10 h). SSCVs were run at a rate of 0.1 mV s^{-1} over a potential range of 2.0–5.0 V versus Li/Li^+ reference electrode. After the first cycle, the cells were held potentio-statically at 3.5 V for 50 h. The cells were then carefully opened in a glove box to recover the spinel electrodes; the electrodes were subsequently rinsed in DMC to remove residual $LiPF_6$ and finally dried in a vacuum oven at 80°C. A Rigaku 2077 X-ray diffractometer was used for the X-ray analyses of the spinel electrodes (Cu Kα).

A Solartron 1287 electrochemical interface with a Solartron 1260 impedance/gain-phase analyzer was used in electrochemical measurements.

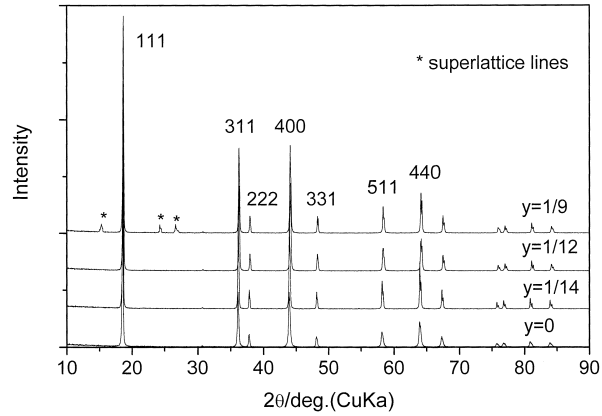

Fig. 1. Powder XRD patterns for $LiAl_yMn_{2-y}O_4$ ($y = 0$, 1/14, 1/12, 1/9).

3. Results and discussion

3.1. XRD study

The XRD patterns of the $LiAl_yMn_{2-y}O_4$ ($y = 0$, 1/14, 1/12, 1/9) are shown in Fig. 1. When the substituted Al content was small, $y \leq 1/12$, the sample was identified as a single spinel phase with the space group, $(Fd\bar{3}m)$, i.e. the observed diffraction lines completely matched those of a cubic spinel $LiMn_2O_4$ structure listed in a JCPDS file, as those of $LiM_yMn_{2-y}O_4$ (M = Cr, Co) [6]. Several new peaks (e.g. $2\theta = 15.1$, 24.4 and 26.6°) appeared for the samples when $y > 1/12$; these refer to a superstructure (space group $P4_332$) formed by ordering of Al and Mn ions in octahedral 16*d* sites [16]. The lattice parameters of the Al-substituted lithium manganese spinels gradually decrease with increasing Al composition (see Table 1).

Fig. 2 shows the XRD patterns of the spinel $LiAl_yMn_{2-y}O_{4-z}F_z$ ($y = 1/12$, $z = 0.012$, 0.033, 0.045) determining the single-phase region. Because new peaks which belong to Li_2MnO_3 were observed at $2\theta = 37.1$ and 44.8° for the sample with $z = 0.045$, the single-phase region of the cubic spinel was estimated to be below 0.04. In Table 2, the lattice parameter *a* was found to increase with increasing fluorine quantity for fixed *y* values. The trend is opposite to what is expected by Vegard's rule for the substitution of O for the smaller F anion. Therefore, the increase in lattice parameter can be assumed to originate in the increase in quantity of the larger trivalent manganese

Table 1
Dependence of the lattice parameter *a* for $LiAl_yMn_{2-y}O_4$ on the Al-substituted composition

$LiAl_yMn_{2-y}O_4$	*a* (Å)
$y = 0$	8.234
$y = 1/14$	8.228
$y = 1/12$	8.219
$y = 1/9$	8.208

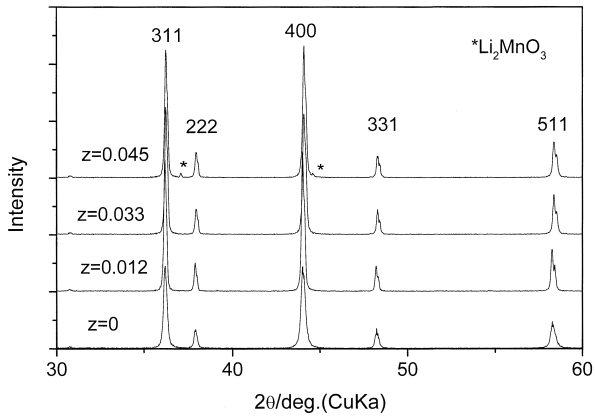

Fig. 2. Powder XRD patterns for $LiAl_yMn_{2-y}O_{4-z}F_z$ ($y = 1/12$, $z = 0$, 0.012, 0.033, 0.045).

Table 2
Dependence of the lattice parameter a for $LiAl_{1/12}Mn_{23/12}O_{4-z}F_z$ on the F-substituted composition

$LiAl_{1/12}Mn_{23/12}O_{4-z}F_z$	a (Å)
$z = 0$	8.219
$z = 0.012$	8.223
$z = 0.033$	8.226

Mn^{3+} (0.79 Å), because of charge compensation relative to the substitution of fluoride ions for oxygen in the structure.

The structure of the substituted spinel is: the lithium ions basically occupy the tetrahedral 8*a* sites, Al and Mn ions in octahedral 16*d* site and F, O ions the 32*e* sites; the 8*b*, 48*f*, and 16*c* sites remain empty.

3.2. Galvanostatic cycle characteristics

Fig. 3 shows the charge–discharge curves at the first cycle for the $Li|LiAl_yMn_{2-y}O_{4-z}F_z$ ($y = 0$, $z = 0$; $y = 1/12$, $z = 0$ and 0.033) cells. The substituted samples seem to maintain uniform cycle shape during intercalation and deintercalation of lithium as observed in $LiMn_2O_4$. The initial discharge capacity of $LiAl_{1/12}Mn_{23/12}O_{4-z}F_z$ ($z = 0.033$) (118 mAh g^{-1}) was 8 mAh g^{-1} higher than that of $LiAl_{1/12}Mn_{23/12}$ O_4 (110 mAh g^{-1}). In $LiAl_{1/12}Mn_{23/12}O_4$, substitution of Mn by Al reduces the capacity of the spinel $LiMn_2O_4$ (127 mAh g^{-1}) in 4 V region since these ions are not oxidized or reduced in this potential range. The increase of the capacity for $LiAl_{1/12}Mn_{23/12}O_{4-z}F_z$ ($z = 0.033$) is due to the reduction of some Mn^{4+} to Mn^{3+} in the formation of the F-substitution. It was shown that the use of monovalent fluorine substitution for divalent oxygen increases the amount of Mn^{3+} content available for redox (thereby increasing specific capacity).

The cycle performance of three samples is shown in Fig. 4. At the 100th cycle, the discharge capacity of the $LiMn_2O_4$ had lost 28% of the initial capacity. On the contrary, the capacity for the Al–F-substituted spinels had maintained more than 92% of the initial capacity at the 100th cycle. Moreover, the Al–F-substituted spinel showed slightly better cycle performance compared with the Al-substituted one. Probably Al–F-substitution would increase the binding energy in the octahedral MO_6 sites, and therefore, contribute to the stabilization of the entire spinel structure.

3.3. Slow speed cyclic voltammetry of spinel: 2–5 V range

The electrochemical behavior and relative stability of $LiM_yMn_{2-y}O_{4-z}F_z$ ($y = 0$, $z = 0$; $y = 1/12$, $z = 0$ and 0.033) during overcharge ($E > 4.5$ V) and overdischarge ($E < 3.5$ V) was examined by SSCV. After 20 cycles were run in 3.5–4.3 V region, voltage limits were expanded to 2 and 5 V (the sweep process: 3.5–5.0–3.5–2.0 V) for two cycles in SSCV shown in Figs. 5–7.

The shape of the first cycle in 3.5–5 V sweep region shows the familiar shape with two pairs of peaks, corresponding to the two-step reversible (de)intercalation of lithium, located at 4.06 (P1) and 4.18 V (P2) on charge and at 3.94 (P3) and 4.07 V (P4) on discharge. The Al–F-substituted spinel shows the greatest peak separation. This may be due to

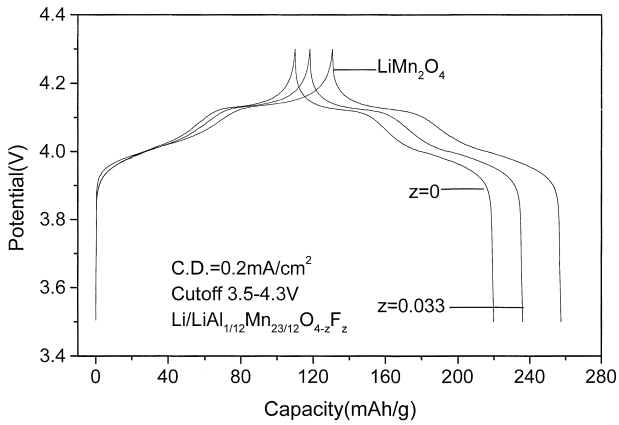

Fig. 3. First charge–discharge curves of $Li/LiMn_2O_4$ and $Li/LiAl_yMn_{2-y}O_{4-z}F_z$ ($y = 1/12$, $z = 0$ and $z = 0.033$) cells.

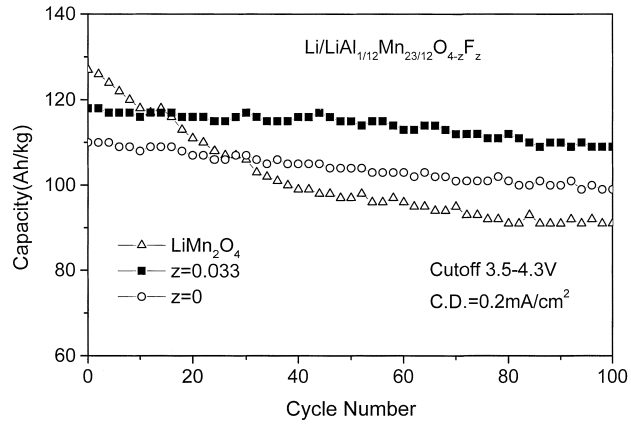

Fig. 4. Cycle performance of $Li/LiMn_2O_4$ and $Li/LiAl_yMn_{2-y}O_{4-z}F_z$ ($y = 1/12$, $z = 0$ and $z = 0.033$) cells.

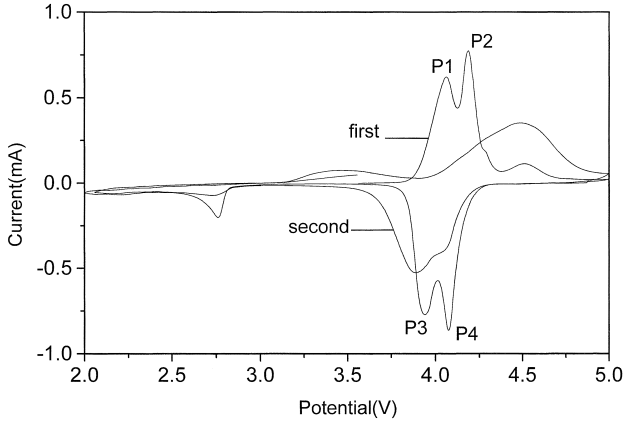

Fig. 5. Cyclic voltammograms of $LiMn_2O_4$ in 1 M $LiPF_6$/(EC + DMC) (1:1) at a sweep rate of 0.1 mV s^{-1}.

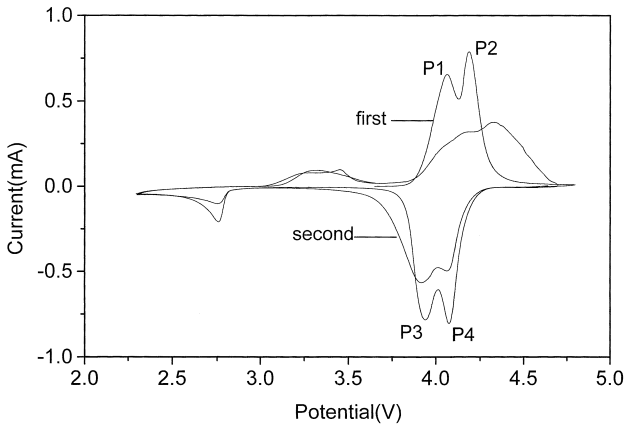

Fig. 6. Cyclic voltammograms of $LiAl_{1/12}Mn_{23/12}O_4$ in 1 M $LiPF_6$/(EC + DMC) (1:1) at a sweep rate of 0.1 mV s^{-1}.

the large concentration of Mn^{3+}, which has been shown to lower the electronic conductivity through a slowing of the electron hopping conduction mechanism [17]. The peaks at 4.5 V observed for $LiMn_2O_4$ did not occur in substituted spinels for the first cycling. This suggested that a small portion of the lithium ions need more energy to be removed from the substituted spinels than $LiMn_2O_4$.

The second cycle of the SSCV is dramatically affected by the sweep to 2 V. The two anodic peaks in $LiAl_{1/12}Mn_{23/12}O_{4-z}F_z$ ($z = 0.033$) collapse into a single broad peak lying at potentials above that of P2, while the cathodic peak point is essentially unchanged. The anodic peak of $LiMn_2O_4$ is broader than that for the substituted spinel. The anodic and cathodic peaks of $LiMn_2O_4$ in 3.5–5 V region are widely separated reflecting the irreversibility of this process at this sweep rate. Electrochemical extraction of one lithium ion from the tetrahedral (8*a*) sites occurs in two steps at approximately 4 V versus Li/Li^+($LiMn_2O_4 \rightarrow Mn_2O_4$ (λ-MnO_2)), whereas the insertion of one lithium ion into the octahedral (16*c*) site occurs at approximately 3 V versus Li/Li^+($LiMn_2O_4 \rightarrow Li_2Mn_2O_4$ ($LiMnO_2$)). The insertion of lithium into $LiMn_2O_4$, towards $Li_2Mn_2O_4$, is naturally accompanied by a reduction of the average oxidation state of manganese from 3.5 to 3: the presence of more than 50% of Jahn–Teller ions (Mn^{3+}) in the host structure introduces a cubic to tetragonal distortion (from $c/a = 1$ to $c/a = 1.16$, $\Delta V/V = 6\%$ [18]), which is believed to hamper the electrical contact between the surfaces of the insertion-material particles and hence to decrease the capacity of the cathode [7]. These results were also confirmed in our experiments by a XRD analysis.

The XRD patterns of spinel cathodes that had been extracted from cells after first SSCV cycle are shown in Fig. 8. The patterns of three cycled electrodes all contain new peaks around $2\theta = 34.4$, 41.0, 60.3 and 61.5°, indicating a trace amount of $Li_2Mn_2O_4$ in the parent compounds [19]. There are two important changes in the XRD patterns. First, for the $LiMn_2O_4$ electrode, the strong peaks at $2\theta = 34.4$ and 41.0° grow significantly in magnitude, indicating an increase in the $Li_2Mn_2O_4$ content in the electrode. Second, compared with the $LiMn_2O_4$, the substituted spinel peaks shift slightly to the right, indicating a contraction of the lattice parameter.

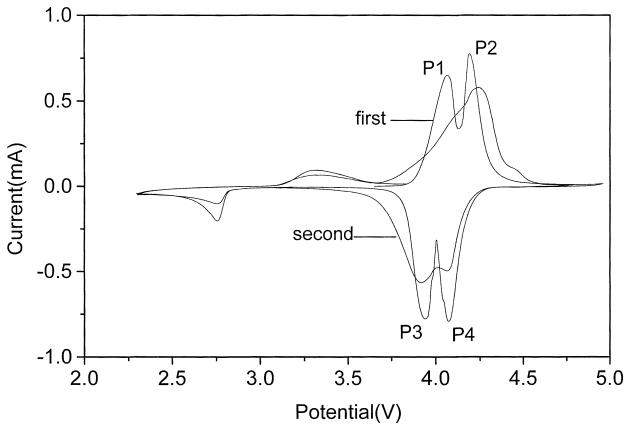

Fig. 7. Cyclic voltammograms of $LiAl_{1/12}Mn_{23/12}O_{4-z}F_z$ ($z = 0.033$) in 1 M $LiPF_6$/(EC + DMC) (1:1) at a sweep rate of 0.1 mV s^{-1}.

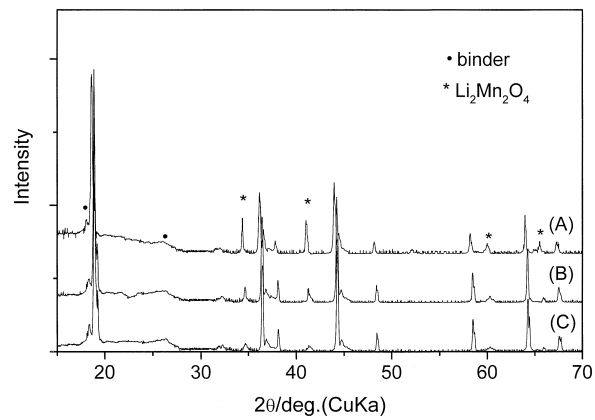

Fig. 8. Powder XRD pattern of spinel electrodes extracted from cells after the first SSCV cycle: (A) $LiMn_2O_4$; (B) $LiAl_yMn_{2-y}O_4$ ($y = 1/12$) and (C) $LiAl_yMn_{2-y}O_{4-z}F_z$ ($y = 1/12$, $z = 0.033$).

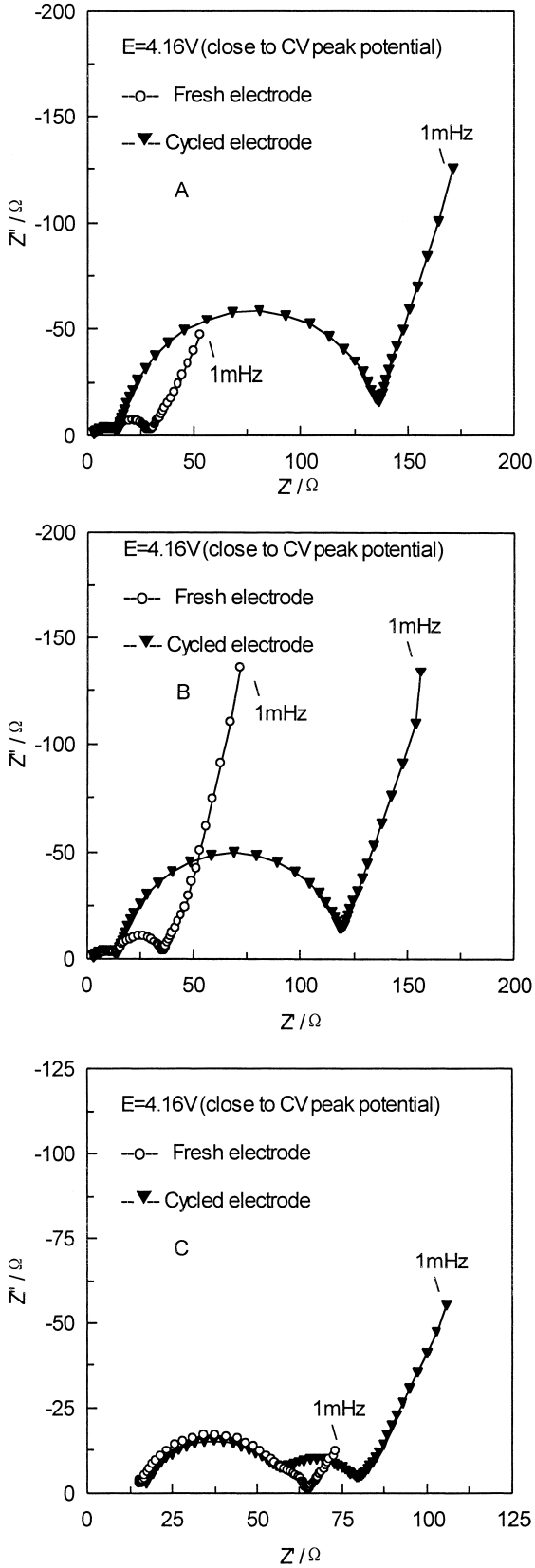

Fig. 9. AC impedance experiments measured for the spinel: (A) Li/$LiMn_2O_4$; (B) Li/$LiAl_yMn_{2-y}O_4$ ($y = 1/12$); (C) Li/$LiAl_yMn_{2-y}O_{4-z}F_z$ ($y = 1/12$, $z = 0.033$) electrodes at the potential $E = 4.16$ V before and after 20 cycles.

From above results, we can conclude that a substituted spinel can suppress the Jahn–Teller instability to improve the cycling performance better than $LiMn_2O_4$.

3.4. EIS characterization

Fig. 9 shows Cole–Cole plots (Nyquist plot: imaginary component, $-Z''$, versus real component, Z') of the ac impedance obtained in ⟨Li/$LiPF_6$/EC + DMC/spinel⟩ half cell. Each compares impedance spectra of the pristine and cycled electrode for three samples, measured at potentials close to the SSCV peak potential, in which the charge-transfer resistance of the electrode is minimal. This figure further demonstrates the impedance changes of these electrodes due to prolonged charge–discharge cycling, which can be correlated with the capacity fading observed. The capacity decrease of these electrodes upon cycling is accompanied by a gradual increase in their charge-transfer resistance. These results demonstrate the SSCV peak potential use of these measurements as an in situ mechanistic tool for characterizing stable behavior versus destructive processes of these electrodes.

During the first and the 20th cycle, prolonged cycling considerably increases the second low-frequency semicircle attributed to the charge transfer of this electrode. The charge-transfer resistance value of the $LiAl_{1/12}Mn_{23/12}O_{4-z}F_z$ ($z = 0.033$) electrode calculated from the second semicircle's diameter increase from ca. 8 to 23 Ω, the $LiAl_{1/12}Mn_{23/12}O_4$ electrode from ca. 22 to 107 Ω, while the $LiMn_2O_4$ electrode increase from ca. 18 to 123 Ω. We propose that the increase in the above parameter of the electrodes during prolonged cycling reflect destructive processes in the active mass, close to the surface films-particle boundary. Initial publications [20,21] with respect to the failure mechanism focused on manganese dissolution rooted in the disproportion of Mn^{3+}. Recently, however, the mechanism has been extended to the ion exchange of H for Li within the tetrahedral 8*a* and octahedral 16*d* sites. The source of H is found in the quantities of HF present in the electrolyte, either from initial contamination or formed by products of side reactions involving the cell components and the electrolyte [22]. Such processes are expected to increase the roughness of the active mass at this boundary. The substituted $LiAl_yMn_{2-y}O_{4-z}F_z$ spinel introduction of an encapsulation concept, where the surface of the spinel is removed from contact with HF-containing electrolyte improves cycle performance of the spinel.

4. Conclusions

Al–F-substituted spinel $LiAl_yMn_{2-y}O_{4-z}F_z$ can compensate for the theoretical capacity reduction in $LiAl_yMn_{2-y}O_4$. The shape of the voltammetric peaks in 2–5 V region and XRD data suggested that F–Al-substituted spinel can suppress the Jahn–Teller instability to improve the cycling

performance better than $LiMn_2O_4$. The above results are further supported by ac impedance experiment. The value of the charge-transfer resistance showed that the substituted $LiAl_yMn_{2-y}O_{4-z}F_z$ spinel introduces an encapsulation concept, where the surface of the spinel is protected from contact with HF containing electrolyte thus improving cycle performance of the spinel.

References

[1] J.M. Tarascon, E. Wang, F.K. Shokoohi, W.R. McKinnon, S. Colson, J. Electrochem. Soc. 138 (1991) 2859.
[2] J.M. Tarascon, D. Guyomard, J. Electrochem. Soc. 138 (1991) 2864.
[3] T. Ohzuku, M. Kitagawa, T. Hirai, J. Electrochem. Soc. 137 (1990) 769.
[4] D. Guyomard, J.M. Tarascon, J. Electrochem. Soc. 139 (1992) 937.
[5] R. Bittihn, R. Herr, D. Hoge, J. Power Sources 43 (1993) 233.
[6] L. Guohua, H. Ikuta, T. Uchida, M. Wakihara, J. Electrochem. Soc. 143 (1996) 178.
[7] R.J. Gummow, A. de Kock, M.M. Thackeray, Solid State Ionics 69 (1994) 59.
[8] A.D. Robertson, S.H. Lu, W.F. Averill, W.F. Howard, J. Electrochem. Soc. 144 (1997) 3500.
[9] A.D. Robertson, S.H. Lu, W.F. Averill, W.F. Howard, J. Electrochem. Soc. 144 (1997) 3505.
[10] F. Le Cras, D. Bloch, M. Anne, P. Strobel, Solid State Ionics 203 (1996) 89.
[11] G. Pistoia, G. Wang, Solid State Ionics 66 (1993) 135.
[12] G.G. Amatucci, A.S. Gozdz, C. Schmutz, F.K. Shokoohi, J.M. Tarascon, Solid State Ionics 86 (1996) 49.
[13] G.G. Amatucci, N. Pereira, T. Zheng, I. Plitz, J.M. Tarascon, J. Power Sources 81 (1995) 39.
[14] Y. Xia, M. Yoshio, J. Power Sources 56 (1995) 61.
[15] T. Ohzuku, J. Kato, K. Sawai, T. Hirai, J. Electrochem. Soc. 138 (1991) 2556.
[16] J. Smith, Geometrical and Structural Crystallography, Wiley, New York, 1982.
[17] I. Saadoune, C. Delmas, J. Solid State Chem. 136 (1998) 8.
[18] M.M. Thackeray, W.I.F. David, P.G. Bruce, J.B. Goodenough, Mater. Res. Bull. 18 (1983) 461.
[19] F. Le Cras, D. Bloch, M. Anne, P. Strobel, Solid State Ionics 89 (1996) 203.
[20] D.H. Jang, J. Shin, S.M. Oh, J. Electrochem. Soc. 143 (1996) 2204.
[21] G.G. Amatucci, C.N. Schmutz, A. Blyr, C. Sigala, A.S. Godzd, D. Larcher, J.M. Tarascon, J. Power Sources 69 (1997) 11.
[22] B. Ammundsen, P.B. Aitchinson, G.R. Buruns, D.J. Jones, J. Roziere, Solid State Ionics 97 (1997) 3342.